Contents lists available at SciVerse ScienceDirect

Inorganica Chimica Acta

A novel route to Pt–Bi$_2$O$_3$ composite thin films and their application in photo-reduction of water

Savio J.A. Moniz [a], Davinder Bhachu [a], Chris S. Blackman [a,b,*], Alison J. Cross [a], Sofia Elouali [a], David Pugh [a], Raul Quesada Cabrera [a], Stella Vallejos [a]

[a] Materials Chemistry Centre, Department of Chemistry, University College London, 20 Gordon Street, London WC1H 0AJ, UK
[b] London Centre for Nanotechnology, 17-19 Gordon Street, London WC1H 0AH, UK

ARTICLE INFO

ABSTRACT

A novel homoleptic bismuth(III) β-diketonate (dibenzoylmethane – dbm) complex [Bi(dbm)$_3$]$_2$ has been used as a precursor to thin films of crystalline β-Bi$_2$O$_3$, and hexachloroplatinic acid (H$_2$PtCl$_6$·6H$_2$O) has been demonstrated as a suitable precursor for deposition of platinum nanoparticles, both deposited *via* aerosol-assisted chemical vapour deposition (AACVD). Thin films of Pt–Bi$_2$O$_3$ were co-deposited from a mixture of [Bi(dbm)$_3$]$_2$ and H$_2$PtCl$_6$·6H$_2$O; the introduction of Pt particles into β-Bi$_2$O$_3$ causes hydrogen to be evolved during photolysis of water over the composite material, a property not found for Pt particles or β-Bi$_2$O$_3$ alone.

© 2011 Elsevier B.V. All rights reserved.

1. Introduction

The ever increasing cost, limited availability and environmental impact of the use of fossil fuels has provided impetus to the search for alternative energy sources that can provide cheap, clean fuel. The use of hydrogen as a renewable chemical fuel source would go some way to decrease greenhouse gas emissions and lessen our dependence on non-renewables [1]. At present, the majority of hydrogen is produced via steam reforming of natural gas, emitting CO$_2$ in the process. An alternative method of hydrogen production is via water splitting, a process which is accompanied by a large increase in free energy as shown in Eq. (1):

$$2H_2O \rightarrow 2H_2 + O_2 \ \Delta G = 238 \text{ kJ mol}^{-1} \tag{1}$$
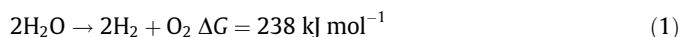
To promote this reaction energy must be input into the system. One of the methods with greatest potential is *via* solar irradiation of a semiconductor, in which the absorbed photons provide the required energy with photo-generated electrons responsible for the reduction of water to H$_2$ and photo-generated holes for the oxidation to O$_2$. The most common materials used for water photolysis are metal oxides because they can be made by low cost routes and are more stable in aqueous environments than non-oxide semiconductors. However many transition metal oxides have band gaps which are too large to serve as efficient water-splitting photo-catalysts under solar irradiation, typically of the order 3.0 eV (Fig. 1), with only ∼5% of the solar spectrum having sufficient energy to produce photo-excited electron/hole pairs.

Bismuth(III) oxide, in which the conduction band is principally Bi 6p in character [2], possesses band gap values of 2.29–3.31 eV depending on the phase present [3], potentially extending the region of the solar spectrum that can be utilised for photo-chemistry into the visible region where more energy is available. Indeed we have recently demonstrated that thin films of β-Bi$_2$O$_3$ are able to photo-oxidise water with high efficiency [4]. For photo-reduction of water however the conduction band potential of bismuth oxide is not sufficient to be able to evolve hydrogen under photo-irradiation (Fig. 1). Various methods exist for modifying the photo-catalytic properties of a semiconductor, for instance the addition of metal particles can act to 'trap' electrons photo-excited in the semiconductor, reducing the overall probability of electron–hole recombination and so increasing the overall efficiency of the photo-system [5]. If made sufficiently reducing by accumulated negative charge these metal particles will readily reduce water to H$_2$ [6]. Therefore one method for obtaining the potential benefit of the relatively narrow band gap of bismuth(III) oxide for solar hydrogen generation would be to combine it with co-catalyst platinum particles.

We have recently demonstrated the co-deposition of metal nanoparticles and a metal oxide using a simple aerosol-assisted chemical vapour deposition (AACVD) method [7]. The use of AACVD has many potential advantages over other methods of producing composite materials, for instance combining materials synthesis and device fabrication in a single step, and it is also a

* Corresponding author at: Materials Chemistry Centre, Department of Chemistry, University College London, 20 Gordon Street, London WC1H 0AJ, UK. Tel.: +44 0 2076794703.
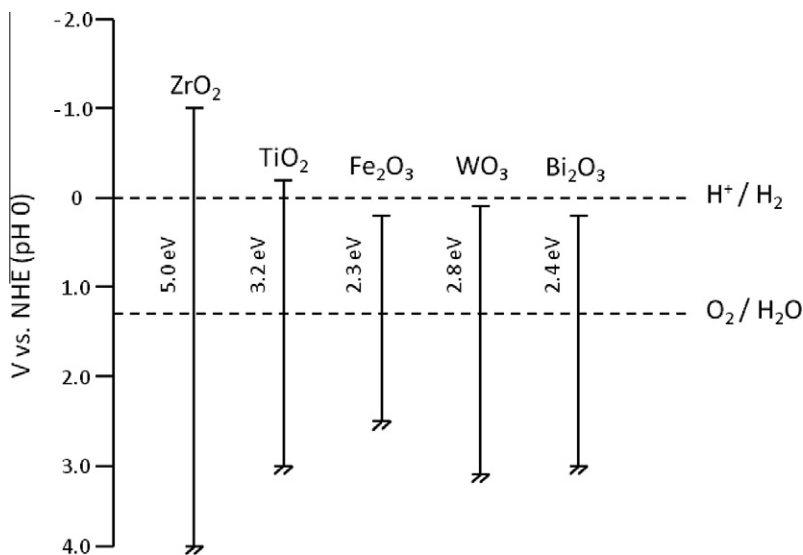E-mail address: c.blackman@ucl.ac.uk (Chris S. Blackman).

Fig. 1. Band structures of some common binary metal oxides and their relationship to the redox potentials of water splitting at pH 0.

relatively low cost technique, with the ability to cover large surface areas with relatively short deposition times. The use of a liquid aerosol to transport reactants in AACVD allows the use of precursors that are not sufficiently volatile or thermally stable for transport in atmospheric or low pressure CVD experiments to be utilised, for instance relatively inexpensive but thermally unstable $HAuCl_4$ was used as the gold precursor in the AACVD co-deposition of tungsten oxide with Au-nanoparticles [7]. Surprisingly, despite the use of $HAuCl_4$ as a precursor to gold nanoparticles *via* AACVD no equivalent chemistry of H_2PtCl_6 has been reported, despite it possessing favourable thermal decomposition characteristics [8].

Unfortunately for the co-deposition of Pt–Bi_2O_3 thin films *via* AACVD H_2PtCl_6 attacks many of the common precursors to bismuth oxide. For instance the donor-functionalised monomeric alkoxide complex [Bi(mmp)$_3$] (mmp = 1-methoxy-2-methyl-2-propanolato) [9] and bismuth *tert*-butoxide [Bi(O^{t}Bu)$_3$] [4] both decomposed in the presence of H_2PtCl_6. Triphenylbismuth is by far the most commonly used bismuth CVD precursor owing to its high air and moisture stability [10,11], however this low reactivity requires the use of a highly reactive oxygen source which is not compatible with the AACVD method. Bismuth tetramethylheptanedionato, [Bi(thd)$_3$]$_2$, has previously been used to deposit bismuth oxide films [12] however it decomposed instantly in solutions containing H_2PtCl_6. The novel homoleptic β-diketonate complex [Bi(dbm)$_3$]$_2$ has been synthesised and structurally characterised, with the complex showing appreciable air and moisture stability and acceptable, although finite, stability in the presence of $H_2PtCl_6 \cdot 6H_2O$. We report the AACVD deposition of thin films of platinum nanoparticles from $H_2PtCl_6 \cdot 6H_2O$, Bi_2O_3 films from [Bi(dbm)$_3$]$_2$ and platinum nanoparticle-modified Bi_2O_3 films from a mixture of [Bi(dbm)$_3$]$_2$ and $H_2PtCl_6 \cdot 6H_2O$. These have been fully characterised and Pt–Bi_2O_3 thin films demonstrated to reduce water to hydrogen under simulated solar irradiation.

2. Experimental procedures

2.1. General procedures

All reactions were performed under a dry, oxygen-free nitrogen atmosphere using standard Schlenk techniques and an MBraun Unilab glove box. Nitrogen (99.996%) was obtained from BOC and used as supplied. Solvents were dried over alumina columns (Anhydrous Engineering) and stored over sodium. All reagents were used without further purification, and were procured from Sigma–Aldrich or Alfa Aesar Ltd.

2.2. Physical measurements

Microanalytical data were obtained at University College London (UCL). NMR spectra were recorded on Bruker AMX 500 machines referenced to C_6D_6 distilled over sodium/benzophenone. ^{1}H and $^{13}C\{^1H\}$ chemical shifts are reported relative to $SiMe_4$ ($\delta = 0.00$ ppm). FT-IR spectra were recorded on a Perkin Elmer Spectrum RX I instrument, over the range 4000–400 cm^{-1}. Mass spectra were recorded on a Micromass ZABSE instrument. Coupled Thermogravimetric Analysis Mass Spectrometry (TGA-MS) was performed on a Netzsh STA 449C instrument using sealed aluminium pans, pierced with a hole at the top prior to heating at atmospheric pressure, under a flow of helium gas (50 sccm); the rate of heating was 10 °C min^{-1}. For single crystal X-ray diffraction crystals were mounted under nitrogen on a glass fibre from Fomblin vacuum oil. Geometric and intensity data were obtained on a Bruker SMART APEX CCD diffractometer using graphite-monochromated Mo Kα radiation ($\lambda_1 = 0.71073$ Å) at 150(2) K. Data reduction and integration was carried out with SAINT+ and absorption corrections applied using SADABS [13]. The solution and refinements were performed using PLATON [14], the WINGX package and all software packages within [15]. Hydrogen atoms were placed in geometrically assigned positions with fixed bond lengths of 0.95 Å. These were refined using a riding model with a $U_{iso}(H)$ value of 1.2 U_{eq} of the parent atom. Wavelength dispersive X-ray spectroscopy (WDX) of the films was performed on a Philips XL30ESEM machine. Scanning electron microscope (SEM) images were obtained on a JSM-6301F Scanning Microscope Field Emission machine after coating samples with an ultrathin layer of gold (not observed in images) to avoid charging. Grazing incidence (5°) powder X-ray diffraction (XRD) was carried out on a Bruker AXS D8 Discover machine using monochromatic Cu Kα radiation ($\lambda_1 = 1.54056$ Å) and a GADDS Area Detector with phase information obtained via the EVA suite of programs (version 2). UV–Vis spectra were recorded in transmission mode over the range 175–2500 nm using a Perkin Elmer Lambda 950 photospectrometer and transmission electron microscopy (TEM) images were captured on a JEOL JEM-100CX II machine operating at 100 kV;

samples were prepared by deposition on KBr substrates followed by dissolution of the substrate in distilled water. XPS spectra were acquired using a Kratos AXIS Ultra machine with a Delay Line Detector. A monochromated Al Kα X-ray source producing a FWHM on the Ag 3d$_{5/2}$ peak of 0.48 eV was utilised, along with a chamber pressure of 7×10^{-9} torr. Samples were etched to 5 and 10 nm in depth for 5 and 10 min respectively.
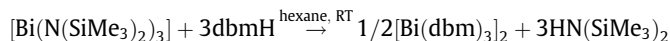
2.3. Synthesis of [Bi(dbm)$_3$]$_2$

Route 1

$$[Bi(Ph_3)] + 3dbmH \xrightarrow[\text{toluene}]{\Delta} 1/2[Bi(dbm)_3]_2 + 3C_6H_6$$
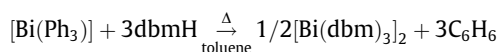
Dibenzoylmethane, (1.53 g, 6.81 mmol) was dissolved in toluene and added drop-wise to triphenylbismuth (1.0 g, 2.27 mmol) dissolved in toluene. The light yellow mixture was heated under reflux for 24 h resulting in a deep yellow solution. Volatiles were removed under vacuum and the resulting solid washed with dichloromethane, filtered and dried under vacuum, leaving behind a yellow crystalline solid (1.57 g, 79%, m.p. 191–198 °C). *Anal.* Calc. for C$_{45}$H$_{33}$O$_6$Bi: C, 61.5; H, 3.79. Found: C, 57.45; H, 3.55%. ^{1}H NMR, δ/ppm (C$_6$D$_6$, 500 MHz): 6.60 (s, 1H, (C*H*)), 7.6 (m, 10H, C$_6$*H*$_5$–). ^{13}C NMR, δ/ppm (C$_6$D$_6$, 500 MHz): 93 (*C*–C=O), 127.8 (2-C$_6$H$_5$), 132.3 (3-C$_6$H$_5$), 133.2 (1-C$_6$H$_5$), 137 (4-C$_6$H$_5$), 185.1 (*C*=O). FT-IR cm^{-1} (KBr disc, Nujol mull): 2924 s, 2957 s, 2857 s, 2722 w, 1806 w, 1599 s, 1588 w, 1538 m, 1510 m, 1463 br s, 1377 versus 1301 m, 1261 m, 1223 m, 1180 m, 1156 w, 1096 br m, 1056 br m, 1021 s, 967 w, 926 m, 800 s, 751 s, 723 versus 693 w, 684 m, 618 m, 608 s, 494 w, 447 s. Mass Spec (CI+, methane): 225 [L]$^+$, 433 [BiL]$^+$, 650 [BiL$_2$]$^+$, 870 [BiL$_3$]$^+$.

Route 2

$$[Bi(N(SiMe_3)_2)_3] + 3dbmH \xrightarrow{\text{hexane, RT}} 1/2[Bi(dbm)_3]_2 + 3HN(SiMe_3)_2$$

A solution of dibenzoylmethane (0.292 g, 1.31 mmol) in hexane was added to a solution of bismuth tris(bis-trimethylsilylamide), [Bi(N(SiMe$_3$)$_2$)$_3$], (0.3 g, 0.435 mmol) in hexane [16]. A yellow precipitate formed almost immediately. The solution was allowed to stir for 24 h at room temperature and then filtered. The bright yellow solid was washed with toluene (2 × 30 cm^3) and dichloromethane (15 cm^3), filtered and dried to leave a free-flowing bright yellow solid (0.32 g, 84%). NMR, IR and elemental analysis were identical to above. Recrystallisation from a concentrated dry dichloromethane solution in a freezer at −18 °C yielded X-ray quality single crystals after 2 days.

2.4. CVD

CVD experiments were performed using a horizontal cold wall CVD reactor previously detailed elsewhere [7]. The substrate temperature was varied between 425 and 525 °C with deposition for 1 h on 25 × 25 mm borosilicate glass or stainless steel (316 grade) substrates. Films of bismuth oxide were deposited using 200 mg of [Bi(dbm)$_3$]$_2$ dissolved in toluene (10 cm^3, not dried), and for films of Pt–Bi$_2$O$_3$ 10 mg of H$_2$PtCl$_6$·6H$_2$O dissolved in 2 cm^3 methanol (not dried) was added to this solution. For platinum-only films 20 mg of H$_2$PtCl$_6$·6H$_2$O was dissolved in 10 cm^3 methanol and the substrate temperature was maintained at 410 °C. In all depositions a nitrogen carrier gas flow of 300 cm^3 min^{-1} was maintained.

2.5. Water photolysis

Hydrogen evolution was measured by illuminating thin film samples suspended in a continuously stirred sacrificial solution with simulated solar irradiation (75 W xenon light source, Photon

Technology International, West Sussex, UK) [17,18]. The solution, which was contained within a silica vessel surrounded by an outer glass water jacket maintained at 20 °C, was composed of a 1:1 mixture of ethanol (acting as a hole scavenger) and water or a 1:1 mixture of ethanol and 0.1 M HCl. Each sample was suspended from a rubber septum which was used to seal the glass vessel to the outside atmosphere. About 250 μL samples of gas were extracted from the headspace of the container hourly via a gas syringe and analysed for hydrogen content using gas chromatography (Varian CP-3800 GC). The GC was calibrated before each experiment using a 250 μL sample of pure hydrogen (BOC).

3. Results and discussion

3.1. Precursor synthesis

There are a number of routes to bismuth(III) β-diketonates reported in the literature. The synthesis of [Bi(thd)$_3$]$_2$ was first reported *via* metathesis of BiCl$_3$ and Na(thd) followed by purification by sublimation [19]. Subsequently it was isolated via reflux of BiPh$_3$ with Hthd [20]. This method has subsequently been applied to the synthesis of a number of bismuth(III) fluorinated β-diketonate complexes including [Bi(fod)$_3$]$_2$ and [Bi(hfac)$_3$]$_2$ (fod = 6,6,7,7,8,8,8-heptafluoro-2,2-dimethyl-3,5-octanedione, hfac = 1,1,1,5,5,5-hexafluoro-2,4-pentanedione) [21], although it proved unsuccessful for synthesis of [Bi(acac)$_3$] [22]. Recently the reaction between [Bi(N(SiMe$_3$)$_2$)$_3$] and Hthd has also been utilised as a route to [Bi(thd)$_3$]$_2$ [16]. The synthetic routes to bismuth(III) β-diketonates are summarized in Scheme 1.

We found that isolation of the pure metallated β-diketonate required for the first of these routes was problematic hence the synthesis of [Bi(dbm)$_3$]$_2$ was attempted *via* the other two routes. Route 1 was *via* refluxing BiPh$_3$ with three molar equivalents of the free ligand, Hdbm, in toluene. Solvent was removed under vacuum to leave [Bi(dbm)$_3$]$_2$ as a bright yellow solid in 79% yield, and the ^{1}H NMR displayed the expected backbone proton resonance at 6.6 ppm and the phenyl peaks at 7.6 ppm. It has been reported that this route is often problematic in synthesising bismuth(III) β-diketonates, with mixed phenyl-diketonate complexes being obtained [21], although the synthesis of [Bi(thd)$_3$]$_2$ has been successful with this methodology [20] and we found it suitable for the preparation of [Bi(dbm)$_3$]$_2$.

Route 2 involved reaction of bismuth silylamide [Bi(N(SiMe$_3$)$_2$)$_3$] with 3 molar equivalents of dbmH in hexane at room temperature for 24 h [16]. Upon addition of the ligand to the amide, it was apparent that the product [Bi(dbm)$_3$]$_2$ immediately precipitated from solution and allowed simple isolation thereafter. The yield in this case was higher than route 1 at 84% and work-up was generally easier and this was the preferred preparative route for this compound.

[Bi(dbm)$_3$]$_2$ is soluble in dichloromethane and toluene and was stored outside of the glove-box for one month, with no appreciable decomposition. Crystals suitable for single-crystal X-ray diffraction
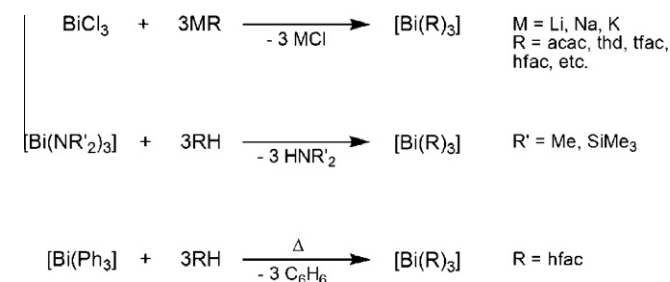
Scheme 1. Synthetic routes to bismuth(III) β-diketonates.

were grown from a concentrated dichloromethane solution after a few days storage at −18 °C. [Bi(dbm)$_3$]$_2$ crystallized in the triclinic space group $P\bar{1}$ as an oxygen-bridged centrosymmetric dimer (Fig. 2).

The inversion point lies at the heart of the Bi$_2$O$_2$ ring at the centre of the molecule. Each bismuth centre is formally 7-coordinate however, with the lone pair on bismuth, there are 8 valence pairs of electrons thus the coordination geometry of [Bi(dbm)$_3$]$_2$ is based on an 8 valence pair compound. The arrangement of electron pairs best fits a square antiprism, with the degree of distortion away from an ideal square antiprism shown in Fig. 3.

Further details on the crystal structure of [Bi(dbm)$_3$]$_2$, including commentary on bond distances and angles compared to other bismuth(III) β-diketonate complexes, are available in the Supplementary information.

3.2. Aerosol-assisted chemical vapour deposition

3.2.1. Bismuth oxide

Deposition of Bi$_2$S$_3$ [23] and Bi$_2$Se$_3$ [24] via AACVD have previously been reported but this technique has not been applied to synthesis of Bi$_2$O$_3$. [Bi(thd)$_3$]$_2$ has been used to deposit bismuth oxide films via liquid-injection CVD but only with oxygen as a co-reactant [12] and [Bi(fod)$_3$]$_2$ has been used for CVD without a co-reactant, however only bismuth films were deposited in this case [21]. In contrast the use of [Bi(dbm)$_3$]$_2$ as a single-source precursor (Thermogravimetric Analysis of [Bi(dbm)$_3$]$_2$ is reported in Supplementary information) deposited yellow, crystalline bismuth oxide films via AACVD on glass and stainless steel substrates over a variety of substrate temperatures between 410 and 525 °C (Table 1); no deposition was observed below 410 °C. Analytical results on both substrates were near identical and hence only the results for deposition on glass are presented below. All films displayed good coverage and were adherent, passing the Scotch tape test but being removed by abrasion with steel wool. No visual changes in the films were noticed after prolonged storage in air.

Film growth rates were ca. 75, 280, 530 and 610 nm h^{-1} at 410, 450, 495 and 525 °C respectively and increased exponentially with increasing temperature with apparent activation energy of 82.7 kJ mol^{-1}. This is somewhat higher than the activation energy
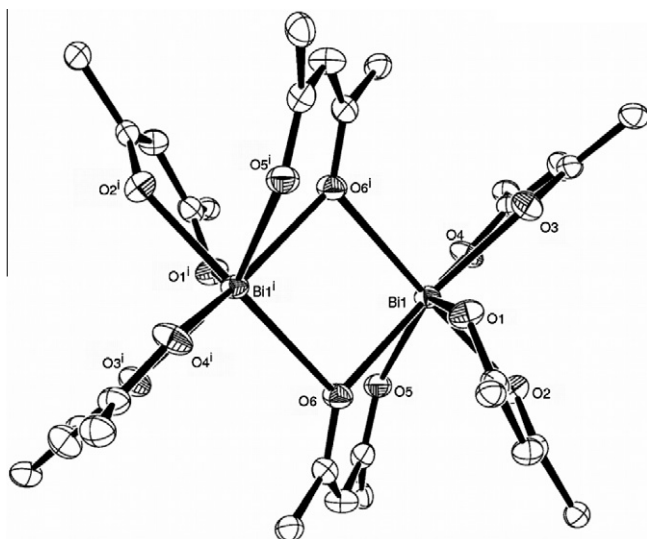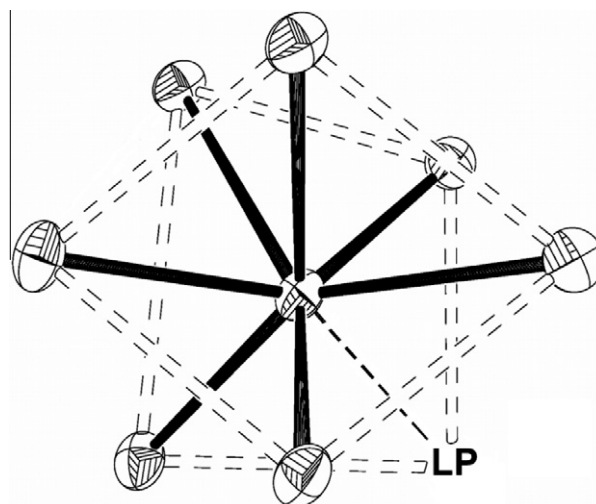

Fig. 3. Diagram representing the 8 valence pairs of electrons around bismuth in a distorted square antiprismatic geometry. LP = stereochemically active lone pair.

Table 1
AACVD film growth conditions for Bi$_2$O$_3$ thin films grown on glass substrates from [Bi(dbm)$_3$]$_2$.

Substrate temperature (°C)	Thickness (nm)	Crystalline phase	Band gap (eV)
410	75	β	2.4
450	280	β	2.4
495	530	β	2.3
525	610	β	2.5

measured for the deposition of α-Bi$_2$O$_3$ films on silicon substrates using [Bi(thd)$_3$]$_2$ as a precursor (62.8 kJ mol^{-1}) using direct-liquid-injection CVD [12], however this is not unexpected due to differences in precursor concentration and mass transport in the two systems. Band-gaps were calculated (for films on glass only) from UV–Vis transmission spectroscopy using Tauc plots [27]. The band gap values fell in the visible range of the spectrum between 2.3 and 2.5 eV and are in good agreement with measured band-gap values obtained for β-Bi$_2$O$_3$ films obtained via LPCVD [4].

Film composition was measured using wavelength dispersive analysis of X-rays (WDX) however bismuth to oxygen ratios could not be determined due to breakthrough to the glass substrate and the presence of carbon contamination could not be ruled out as the insulating nature of the films required coating before analysis, preventing accurate determination of carbon content. The X-ray diffraction pattern of a Bi$_2$O$_3$ film deposited on glass at 450 °C is shown in Fig. 4. All peaks can be matched to β-Bi$_2$O$_3$, and the tetragonal unit cell parameters are in agreement with literature values [25] ($\alpha = \beta = 7.72(2)$ Å, $\gamma = 5.62(2)$ Å, JCPD Card No. 027-0050), with similar results found across the temperature range examined.

SEM (Fig. 5) of a Bi$_2$O$_3$ film deposited on glass at 450 °C displays a globular morphology containing spherical bismuth oxide particles that are approximately 80 nm in diameter. This morphology is quite different to that observed for β-Bi$_2$O$_3$ films obtained via LPCVD which had non-uniform grains composed of triangular crystallites [4], although it is consistent with morphologies seen for AACVD deposited oxide thin films [26].

Fig. 2. ORTEP diagram showing the dimeric nature of [Bi(dbm)$_3$]$_2$. Thermal ellipsoids at 50% probability, phenyl rings (bar ipso carbons), one CH$_2$Cl$_2$ solvent of crystallization and hydrogen atoms omitted for clarity. Atoms labelled 'i' are related by the symmetry code $1 − x$, $1 − y$, $1 − z$.

3.2.2. Platinum

We found the optimum temperature for deposition of platinum(0) films to be 410 °C. Platinum films were adherent to the
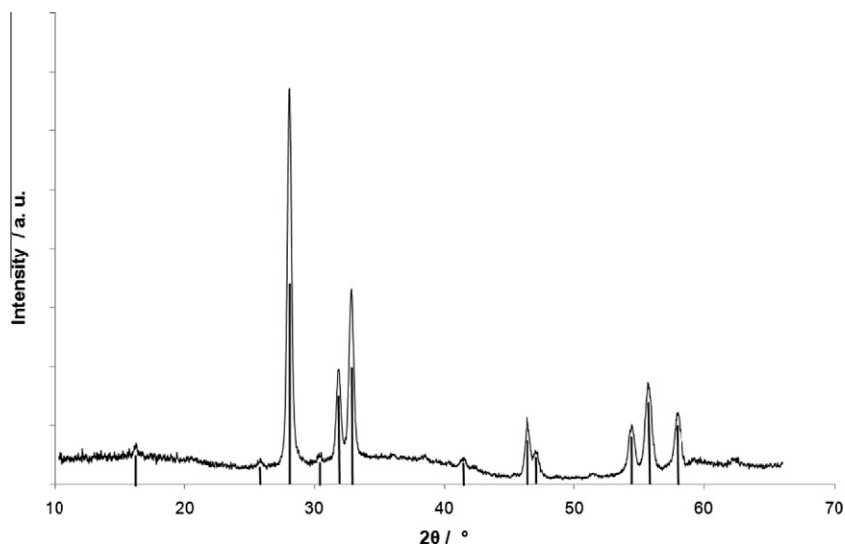
Fig. 4. XRD pattern of film deposited at 450 °C on a glass substrate; reflection planes for β-Bi₂O₃ (JCPD Card No. 027-0050) shown.
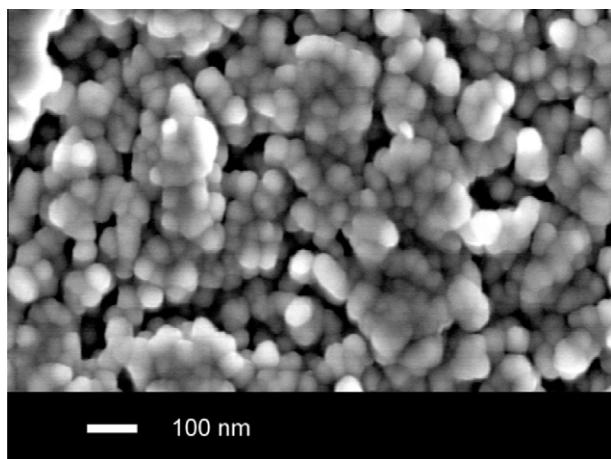

Fig. 5. SEM micrograph of a Bi₂O₃ film deposited at 450 °C on a glass substrate showing globular morphology.

substrate however they could be removed with mild abrasion. WDX analysis revealed chlorine contamination within the films to be negligible (less than 1 at.%). An XRD pattern of a platinum film deposited at 410 °C on glass is shown in Fig. 6 and consists of only two peaks, assigned to platinum metal (JCPD Card No. 004-0802); the low signal to noise ratio and high background between 20° and 30° 2θ is due to the glass substrate.

SEM imaging of a platinum film deposited at 410 °C (Fig. 7) reveals a morphology consisting of particles approximately 200–400 nm in diameter alongside smaller features roughly 100 nm diameter.

To prepare samples for TEM analysis depositions were performed on KBr substrates. XRD, SEM and WDX were consistent with results obtained during deposition on glass. The disc was dissolved in distilled water to remove KBr, leaving the platinum behind for imaging. The TEM image (Fig. 8) shows individual, well-defined platinum particles of approximately 4–10 nm in size whilst estimation of the particle size from XRD data (Scherrer equation) gave a value of ∼10 nm. These results suggest the features observed in SEM (Fig. 7) are agglomerates of Pt nanoparticles.
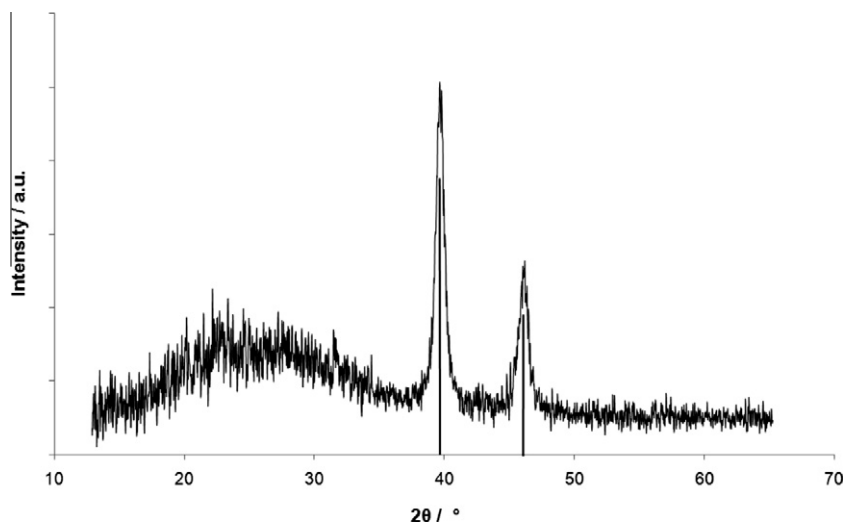

Fig. 6. XRD pattern of a film deposited at 410 °C on a glass substrate; reflection planes for Pt (JCPD Card No. 004-0802) highlighted.
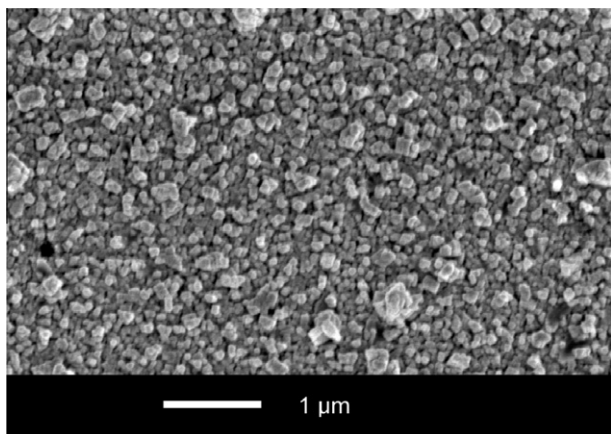
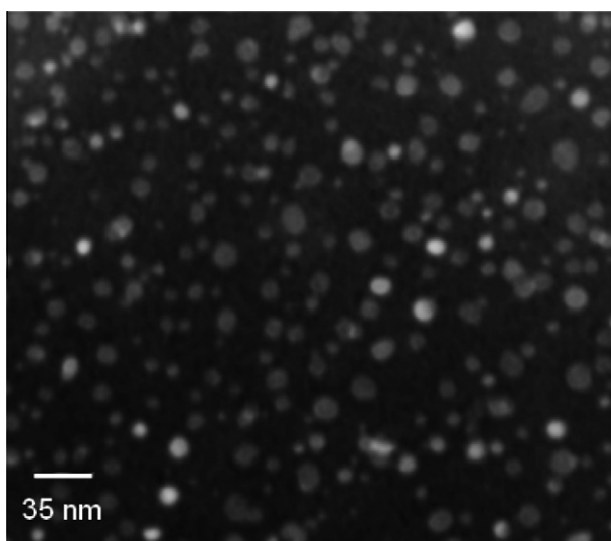**Fig. 7.** SEM image of a platinum film deposited at 410 °C on a glass substrate.

Fig. 8. TEM image of platinum nanoparticles deposited at 410 °C on a KBr substrate.

3.2.3. Co-deposited platinum and bismuth oxide

Pt–Bi_2O_3 films were obtained from co-deposition of $[Bi(dbm)_3]_2$ and $H_2PtCl_6 \cdot 6H_2O$ on steel substrates at 450 °C. WDX analysis showed the films were slightly oxygen deficient (stoichiometry $Bi_2O_{2.8}$) which is similar to β-Bi_2O_3 films found in the literature [4] and they contained an average of 0.36 at.% Pt in $Bi_2O_{2.8}$ (0.89 at.% as a fraction of bismuth only). Chlorine contamination was negligible (<1 at.%) in these films, which is somewhat surprising given the heavy chlorine contamination observed when using glass as a substrate Supplementary information),and as a result the concomitant formation of BiOCl was not observed for samples deposited on steel. The cause of this variability is not immediately obvious, particularly given that results for deposition of Bi_2O_3-only thin films were nearly identical irrespective of the substrate used.

X-ray diffraction (Fig. 9) of the films deposited on stainless steel revealed the presence of β-Bi_2O_3 as the dominant crystalline phase. Unit cell parameters were consistent with the values obtained for deposition of Bi_2O_3-only and are in agreement with literature values {$\alpha = \beta = 7.77(2)$ Å, $\gamma = 5.65(2)$ Å, JCPD Card No. 027-0050} [25]. The high, rising background observed in the pattern is due to fluorescence of the iron atoms present in the steel. Substrate peaks were clearly identified in the X-ray patterns, with no secondary phases of bismuth oxide and no peaks corresponding to platinum(0) observed. The lack of peaks for platinum is perhaps not

surprising given the relatively low amount of platinum present in these Pt–Bi_2O_3 samples (0.36 at.% based on $Bi_2O_{2.8}$).

SEM showed the films to be composed of globular particles similar to those obtained for Bi_2O_3-only samples (Fig. 5) and TEM (of samples deposited on KBr substrates) showed individual disperse platinum nanoparticles, with average diameter of 5 nm or less, visible on the surface of much larger bismuth oxide crystallites. No equivalent features were observed in TEM of Bi_2O_3-only samples.

The composition of a Pt–Bi_2O_3 film deposited at 450 °C on stainless steel was studied using X-ray Photoelectron Spectroscopy. From the surface scan the bismuth $4f_{7/2}$ ionisation was at 158.9 eV and the O1s ionisation at 529.6 eV, both of which are characteristic of Bi_2O_3 [28]. The ratios of the areas of these peaks revealed slightly sub-stoichiometric $Bi_2O_{2.7}$, which is consistent with WDX analysis and is commonly found in β-Bi_2O_3 due to oxygen vacancies in the lattice [10]. Two distinct platinum peaks were observed at 71.5 (Pt $4f_{7/2}$) and 74.8 (Pt $4f_{5/2}$) eV which are characteristic of platinum(0) [29] and rule out formation of $PtCl_2$ or PtO_x [30]. This ionisation is not ascribed to $Pt(OH)_2$ as the Pt $4f_{7/2}$ ionisation would be expected at significantly higher energy (72.4 eV [30]) and the XRD of a Pt-only film deposited at 410 °C (Fig. 6) shows formation of platinum metal, hence we conclude the platinum is present in the Pt–Bi_2O_3 films as platinum metal. Carbon contamination was significant on the surface (~25 at.%) but decreased upon etching (~15 at.% after ~10 nm), however due to preferential sputtering quantification becomes unreliable and extensive etching was not performed.

AFM gave a value for root mean squared roughness (rms) of 97 nm. This is similar to reported values of indium–gallium oxide films formed via AACVD [26] but much higher than films of β-Bi_2O_3 (rms = 4.1 nm) deposited via low-pressure CVD [4]. The relatively high surface area obtained via AACVD is expected to be advantageous for catalytic purposes by giving a high contact area with the surrounding medium.

3.3. Water photolysis

Water photolysis was conducted using Bi_2O_3 and Pt–Bi_2O_3 samples deposited on stainless steel at 450 °C, with films of Pt deposited via AACVD and TiO_2 (anatase) deposited via atmospheric pressure CVD [31], both on stainless steel substrates, used to provide comparison (Table 2). Measurements were made in a sacrificial solution comprised of a 1:1 mixture of ethanol and water (results for a 1:1 mixture of ethanol and 0.1 M HCl are given in Supplementary information).

As expected non-platinised Bi_2O_3 samples produced no hydrogen upon illumination; it is apparent from Fig. 1 that the conduction band of Bi_2O_3 is too low in energy to reduce water to hydrogen at pH 0 and the use of a solution with near neutral pH is expected to exacerbate this problem. In fact this is the likely reason that no H_2 evolution is observed for the TiO_2 sample, despite the fact H_2 evolution was observed from the solution containing HCl (Supplementary information), with the evolution of H_2 becoming increasing thermodynamically unfavourable with increasing pH. No hydrogen evolution was observed over Pt films however Pt–Bi_2O_3 thin films produced an average of 3.1 μmol H_2 h^{-1} m^{-2}. This represents an apparent quantum efficiency of 0.6% (at 420 nm) and is of the order of those obtained using powdered catalysts CdS–ZnS and Pt–TaON:Pt–WO_3 [32]. Although the rate of H_2 evolution is low it should be highlighted these films have not been optimised in terms of film thickness or platinum loading. Previously it has been suggested that β-Bi_2O_3 is unstable to conversion to α-Bi_2O_3 under photo-irradiation [33] but we observed no visual degradation of any of the Bi_2O_3 or Pt–Bi_2O_3 samples during repeated irradiation in the ethanol:water solution and XRD analysis of films after photocatalytic testing showed the only phase present was
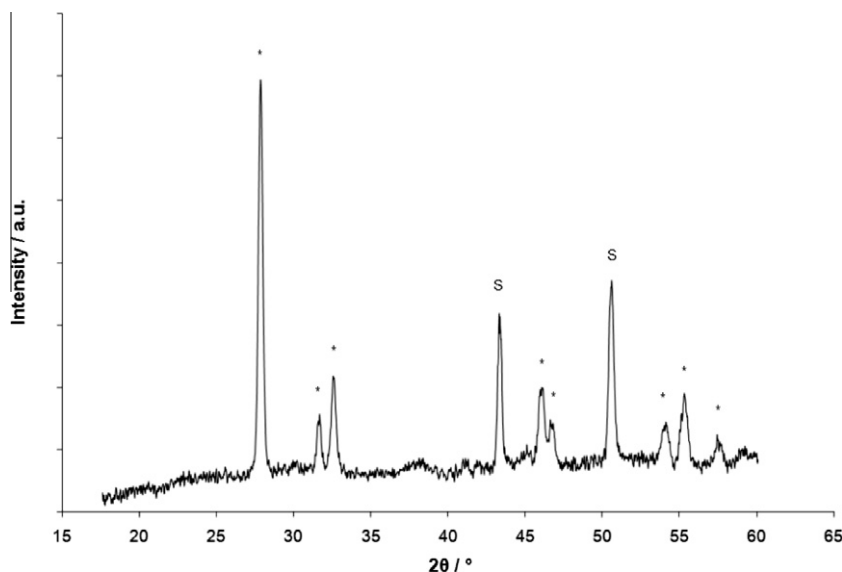
Fig. 9. X-ray diffraction pattern of Pt–Bi_2O_3 film deposited at 450 °C on a stainless steel substrate. Asterisks ($*$) refer to β-Bi_2O_3 peaks whereas peaks marked S correspond to the steel substrate.

Table 2
Rates of H_2 evolution on irradiation of samples immersed in 1:1 solution of ethanol and water.

Material	Rate of H_2 production (μmol h^{-1} m^{-2})
Pt	0
Bi_2O_3	0
Pt–Bi_2O_3	3.1
TiO_2	0

β-Bi_2O_3, hence we conclude under these conditions β-Bi_2O_3 is photostable.

Neither thin films of platinum nanoparticles or of β-Bi_2O_3 evolved H_2 during water photolysis, therefore the ability of composite Pt–Bi_2O_3 to photo-reduce water is a property not contained by the constituent components. There is currently great interest in plasmon resonance enhancement of semiconductor photo-catalytic performance [34] and recently powdered Pt–Bi_2O_3 has been shown to be a highly active catalyst for photo-oxidation [35]. This has been ascribed to plasmonic enhancement of the photo-reaction, despite the fact that platinum nanoparticles have not previously been reported to have plasmonic properties. Plasmon enhancement causes increased light absorption, i.e. potentially increased quantum efficiency, but would not affect the thermodynamic potential of the Bi_2O_3 conduction band and therefore this effect alone would not be expected to enable photo-reduction of water over Pt–Bi_2O_3. We conclude the mechanism for the evolution of hydrogen must be *via* photon capture in the Bi_2O_3 followed by electron transfer to the Pt particles where they are trapped, this charge accumulates until the Pt particles become reducing [6].

4. Conclusions

We have synthesised a novel, moisture stable homoleptic bismuth(III) β-diketonate complex [Bi(dbm)$_3$]$_2$ which has been used as a single-source precursor to bismuth oxide films *via* AACVD. We have reported the use of $H_2PtCl_6 \cdot 6H_2O$ as a precursor to platinum nanoparticles *via* AACVD and we have demonstrated its use via co-deposition in conjunction with [Bi(dbm)$_3$]$_2$ to deposit thin films of platinum nanoparticle-doped bismuth oxide *via* AACVD. The Pt–Bi_2O_3 composite films photo-reduced water under simulated solar irradiation, which is attributed to photon capture within the Bi_2O_3 followed by electron transfer to the Pt nanoparticles upon which the water reduction occurs.

Appendix A. Supplementary material

CCDC 837634 contains the supplementary crystallographic data for this paper. These data can be obtained free of charge from The Cambridge Crystallographic Data Centre via www.ccdc.cam.ac.uk/data_request/cif. Supplementary data associated with this article can be found, in the online version, at doi:10.1016/j.ica.2011.09.029.

References

[1] A. Bard, M. Fox, Acc. Chem. Res. (1995) 141.
[2] A. Walsh, G. Watson, D. Payne, R. Edgell, J. Guo, P.-A. Glans, T. Learmonth, K. Smith, Phys. Rev. B 73 (2006) 1.
[3] L. Leontie, Surf. Sci. 507–510 (2002) 480.
[4] S.J.A. Moniz, C.S. Blackman, C.J. Carmalt, G. Hyett, J. Mater. Chem. 20 (2010) 7881.
[5] P.V. Kamat, J. Phys. Chem. C 111 (2007) 2834.
[6] A. Mills, S.K. Lee, Platin. Met. Rev. 47 (2003) 2.
[7] S. Vallejos, T. Stoycheva, P. Umek, C. Navio, R. Snyders, C. Bittencourt, E. Llobet, C. Blackman, S. Moniz, X. Correig, Chem. Commun. 47 (2011) 565.
[8] A. Schweizer, G. Kerr, Inorg. Chem. 17 (1978) 2326.
[9] P.A. Williams, A.C. Jones, M.J. Crosbie, P.J. Wright, J.F. Bickley, A. Steiner, H.O. Davies, T.J. Leedham, G.W. Critchlow, Chem. Vap. Deposition 7 (2001) 205.
[10] G. Bandoli, D. Barreca, E. Brescacin, G.A. Rizzi, E. Tondello, Chem. Vap. Deposition 2 (1996) 238.
[11] C. Bedoya, G.G. Condorelli, G. Anastasi, A. Baeri, F. Scerra, I.L. Fragalà, J.G. Lisoni, D. Wouters, Chem. Mater. 16 (2004) 3176.
[12] S. Kang, Thin Solid Films 468 (2004) 79.
[13] Bruker, SMART, SAINT and SADABS. Bruker AXS Inc., Madison, Wisconsin, USA, Version 2 (2006).

[14] P. Van der Sluis, A.L. Spek, Acta Crystallogr., Sect. A 46 (1990) 194.
[15] L.J. Farrugia, J. Appl. Crystallogr. 32 (1999) 83.
[16] T. Hatanpää, M. Vehkamäki, M. Ritala, M. Leskelä, Dalton Trans. (Cambridge, England: 2003) 39 (2010) 3219.
[17] G. Hyett, J.A. Darr, A. Mills, I.P. Parkin, Chem. Vap. Deposition 16 (2010) 301.
[18] S. Elouali, A. Mills, I.P. Parkin, E. Bailey, P.F. McMillan, J.A. Darr, J. Photochem. Photobiol., A 216 (2010) 110.
[19] M.-C. Massiani, R. Papiernik, L.G. Hubert-Pfalzgraf, J.-C. Daran, Polyhedron 10 (1991) 437.
[20] L. Armelao, G. Bandoli, M. Casarin, G. Depaoli, E. Tondello, A. Vittadini, Inorg. Chim. Acta 276 (1997) 340.
[21] K.C. Brooks, S.B. Turnipseed, R.M. Barkley, R.E. Sievers, J.V. Tulchinsky, A.E. Kaloyerosj, Chem. Mater. (1992) 912.
[22] A. Pisarevsky, in: AIP Conference Proceedings, 1992, p. 231.
[23] J. Waters, D. Crouch, J. Raftery, P. O'Brien, Chem. Mater. 16 (2004) 3289.
[24] A.A. Tahir, M.A. Ehsan, M. Mazhar, K.G.U. Wijayantha, M. Zeller, A.D. Hunter, Chem. Mater. 22 (2010) 5084.
[25] H.A. Harwig, Z. Anorg. Allg. Chem. 444 (1978) 151.
[26] C.E. Knapp, G. Hyett, I.P. Parkin, C.J. Carmalt, Chem. Mater. (2011) 1719.
[27] J. Tauc, R. Grigorovici, A. Vancu, Phys. Status Solidi B 15 (1966) 627.
[28] V.S. Dharmadhikari, S. Sainkar, S. Badrinarayan, A. Goswami, J. Electron Spectrosc. Relat. Phenom. 25 (1982) 181.
[29] T. Morikawa, T. Ohwaki, K.-ichi Suzuki, S. Moribe, S. Tero-Kubota, Appl. Catal., B 83 (2008) 56.
[30] J. Hammond, N. Winograd, J. Electroanal. Chem. Interf. Electrochem. 78 (1977) 55.
[31] G. Hyett, J.A. Darr, A. Mills, I.P. Parkin, Chem. – A. Eur. J. 16 (2010) 10546.
[32] A. Kudo, Y. Miseki, Chem. Soc. Rev. 38 (2009) 253.
[33] Y. Wang, Y. Wen, H. Ding, Y. Shan, J. Mater. Sci. 45 (2009) 1385.
[34] Z. Liu, W. Hou, P. Pavaskar, M. Aykol, S.B. Cronin, Nano Lett. 11 (2011) 1111.
[35] R. Li, W. Chen, H. Kobayashi, C. Ma, Green Chem. 12 (2010) 212.